Journal of Mammalian Evolution (2024) 31:6
https://doi.org/10.1007/s10914-023-09698-w

RESEARCH

New materials of *Pliorhinus ringstroemi* from the Linxia Basin (Late Miocene, eastern Asia) and their taxonomical and evolutionary implications

Shijie Li[1,2] · Oscar Sanisidro[3] · Shiqi Wang[1,2] · Rong Yang[4] · Tao Deng[1,2]

Accepted: 14 November 2023 / Published online: 29 January 2024

Abstract
A large collection of dicerorhine rhinoceros remains, here identified as *Pliorhinus ringstroemi*, were studied from the Late Miocene deposits of the Linxia Basin, eastern Asia. The new specimens include several complete skulls with for the first-time preserved premaxillae, providing new knowledge on the morphology and allowing a preliminary investigation of the intraspecific variation of the species. The morphological study supports *Pliorhinus ringstroemi* as a valid species and phylogenetic analyses place it as the sister group of *P. megarhinus* and *P. miguelcrusafonti*. Compared with *P. megarhinus*, the unique characters of *P. ringstroemi* include the better developed and oval I1, tusk-like i2, complex secondary folds on upper cheek teeth, convex base of the mandibular corpus, and slightly different skull shape as supported by the geometric morphometric study. Our findings confirm the gradual reduction of incisors, elongated nasal, retracted nasal notch, and, finally, a developed bony nasal septum previously reported for Dicerorhina. The early age and primitive traits suggest that *Pliorhinus* could have originated in Asia and migrated to Europe at the latest Miocene, taking the niche of closely related species *Dihoplus pikermiensis* in Europe.

Keywords Late Miocene · Linxia Basin · Phylogeny · *Pliorhinus ringstroemi* · Rhinocerotidae

Introduction

The Late Miocene is an important period for the rise and initial radiation of several crown groups for mammals at the family level, e.g., Felidae (Johnson et al. 2006; Li et al. 2016), Canidae (Tedford et al. 2009), Cervidae (Gilbert et al. 2006), and some tribes of Bovidae (Bibi 2013). Rhinocerotini is also one of them, with multiple species closely related to modern genera being first recorded by that time. Two genera were commonly seen in northern Eurasia during the late Late Miocene (Turolian of Europe and Baodean in eastern Asia), i.e., *Dihoplus* and *Miodiceros* (Ringström 1924; Deng 2006; Giaourtsakis 2022). Both genera are large in size, slightly smaller than the modern *Ceratotherium simum* in skull length (Ringström 1924; Guérin 1980; Antoine and Saraç 2005). *Miodiceros* is so far only known from the western part of Eurasia, whereas *Dihoplus* is more widely spread over northern Eurasia.

In eastern Asia, the first recognition of *Dihoplus* (as *Dicerorhinus orientalis*) was from Baode, Shanxi Province, and Xin'an, Henan Province, northern and central China (Ringström 1924). These materials were later erected as a new variety *Dic. orientalis* var. *ringströmi* by Arambourg (1959). This form was later elevated to the species level (Chen and Wu 1976) based on significant differences between the eastern Asian species and *Dih. pikermiensis*, a taxonomic opinion later followed by many subsequent authors (Deng 2006; Tong 2012). Several new skulls of *Dic. ringstromi* were later reported from the Linxia Basin (Deng 2006). The genus *Dihoplus* was resurrected for these Late Miocene large dicerorhines by Groves (1983) under the

✉ Tao Deng
dengtao@ivpp.ac.cn

1 Key Laboratory of Vertebrate Evolution and Human Origins of Chinese Academy of Sciences, Institute of Vertebrate Paleontology and Paleoanthropology, Chinese Academy of Sciences, Beijing 100044, China

2 University of Chinese Academy of Sciences, Beijing 100049, China

3 GloCEE - Global Change Ecology and Evolution Research Group, Departamento Ciencias de la Vida, Universidad de Alcalá, Madrid 28805, Spain

4 Hezheng Paleozoological Museum, Hezheng 731200, China

binomen *Dihoplus ringstroemi* (not *ringstromi*, as "ö" should be latinized as "oe"), and followed by most later authors (Heissig 1999; Giaourtsakis 2003; Deng et al. 2011). However, the validation of this species was recently challenged by Pandolfi et al. (2015). They regarded the differences between eastern Asian materials and *Dih. pikermiensis* proposed by Arambourg (1959), Deng (2006), and Tong (2012) as valid, but largely overlapping with the differences between *Dih. pikermiensis* and *Dih. megarhinus* (a latest Miocene to Early Pliocene species that was largely overlooked in the comparisons included in Deng 2006 and Tong 2012). As a consequence, Pandolfi et al. (2015) synonymized *Dih. ringstroemi* with *Dih. megarhinus* due to their similarity. Later, Pandolfi et al. (2021) erected a new genus, *Pliorhinus*, for *Dih. megarhinus* and transferred the Late Miocene material from eastern Asia to *P. megarhinus*. However, even though skulls and mandibles have been discovered in eastern Asian materials, some key anatomical structures (e.g., premaxillary and mandibular morphologies) have been unknown up to now. Moreover, the variability of many traits remains unexplored, which hampers a more reliable discussion on taxonomy. Our phylogeny (detailed below) suggests that *Dih. ringstroemi* should be reconsidered as a valid species of *Pliorhinus*.

The Linxia Basin in the northeastern border of the Tibetan Plateau has produced one of the richest Cenozoic fossil assemblages from the Oligocene to Quaternary in the world (Deng 2009; Deng et al. 2013a, b). In the basin, the Late Miocene deposits are the most fossiliferous ones. Several new skulls of *Dih. ringstroemi* have been reported from the Linxia Basin, but only one nearly undeformed skull has been described and figured (Deng 2006). In the past 15 years, new remains of this species have been gradually collected and prepared. These include complete adult skulls with well-preserved premaxillae, and juvenile crania. These materials are crucial for clarifying the taxonomic position of eastern Asian species and studying the phylogenetic position of the species.

Institutional abbreviations **HM** Hezheng Paleozoological Museum, Hezheng, China; **IVPP** Institute of Vertebrate Paleontology and Paleoanthropology, Chinese Academy of Sciences, Beijing, China; **PMU** Uppsala University, Uppsala. Sweden.

Anatomical Abbreviations M/m, upper/lower molar; P/p, upper/lower premolar.

Materials and methods

The materials described in this study include five complete or nearly complete skulls (one with an associated mandible) of adult individuals and a juvenile skull with a mandible currently housed at Hezheng Paleozoological Museum, Hezheng, China. Two adult skulls that preserve the premaxillae likely have a dorso-ventral compression, the other three individuals are nearly undeformed. These skulls were collected from the top red clay of the Liushu Formation at Zhuangheji, Qianzhuang, Jinchanggou, and Heilingding, Linxia Basin (Fig. 1). The juvenile skull is from an unclear locality in the Linxia Basin. Localities at the top of the Liushu Formation belong to the Qingbushan Fauna and indicate a Baodean Age. The Qingbushan horizon is within chron C3An.2n of the geomagnetic polarity time scale, with an age of ~6.5 Ma (Deng 2006; Deng et al. 2013a, b).

For cranial measurements and anatomical terms, we follow those of Deng (2004), Antoine and Saraç (2005), and Qiu and Wang (2007). Linear measurements were made either with a caliper (dentition) or using Artec Studio 14 Professional and 3D models for crania and mandibles (we have tested that both methods give very similar results). The measurement results are shown in Tables 1, 2 and 3.

Data for geometric morphometric analyses of the dorsal and lateral views were obtained using tpsDig 2.3.2 (Rohlf 2010) and were analyzed using the R package geomorph 4.0.1 (Adams and Otárola-Castillo 2013; Baken et al. 2021). Three curves (with semilandmarks equal distance within each curve) and 10 landmarks are selected in the lateral view, and three curves are selected in the dorsal view (See Online Resource 1 for details, and Online Resource 2–4 for data and R-codes). The datapoint were then superposed by Procrustes analyses, and the relative warp analyses were then performed. Statistical plots were made using the R package ggplot2 (Wickham 2016).

We performed a phylogenetic analysis based on the matrix published by Pandolfi (2023). The coding of *P. ringstroemi* is based on our new specimens and previously published specimens from the Xin'an, Baode, and the Linxia basins (Ringström 1924; Arambourg 1959; Deng 2006).

Bayesian inference with tip-dating (Ronquist et al. 2012a) under the fossilized birth-death model (Zhang et al. 2016) was implemented to infer the phylogeny of Rhinocerotidae. The fossilized birth-death model can incorporate various parameters in phylogenetic inference, especially the age of each taxon. MrBayes 3.2.6 (Huelsenbeck and Ronquist 2001; Ronquist et al. 2012b) was used for the analyses. The ages of the fossil species (see Online Resource 5 for details) follow those published by Heissig (1999), Pandolfi et al. (2021), and Deng (2006). Two independent runs with four chains each were run 10 million times. The first 25% of the results were discarded as 'burn-in'. Traits 1–67, 69–88, 90–96, 98–130, 132–178, 180–264, 266–280 were viewed as additive following Pandolfi (2023), and all traits were treated with equal weight. Recent genomic research on modern and extinct rhinos has shed light on the evolution of the group. Here, we use the results of the

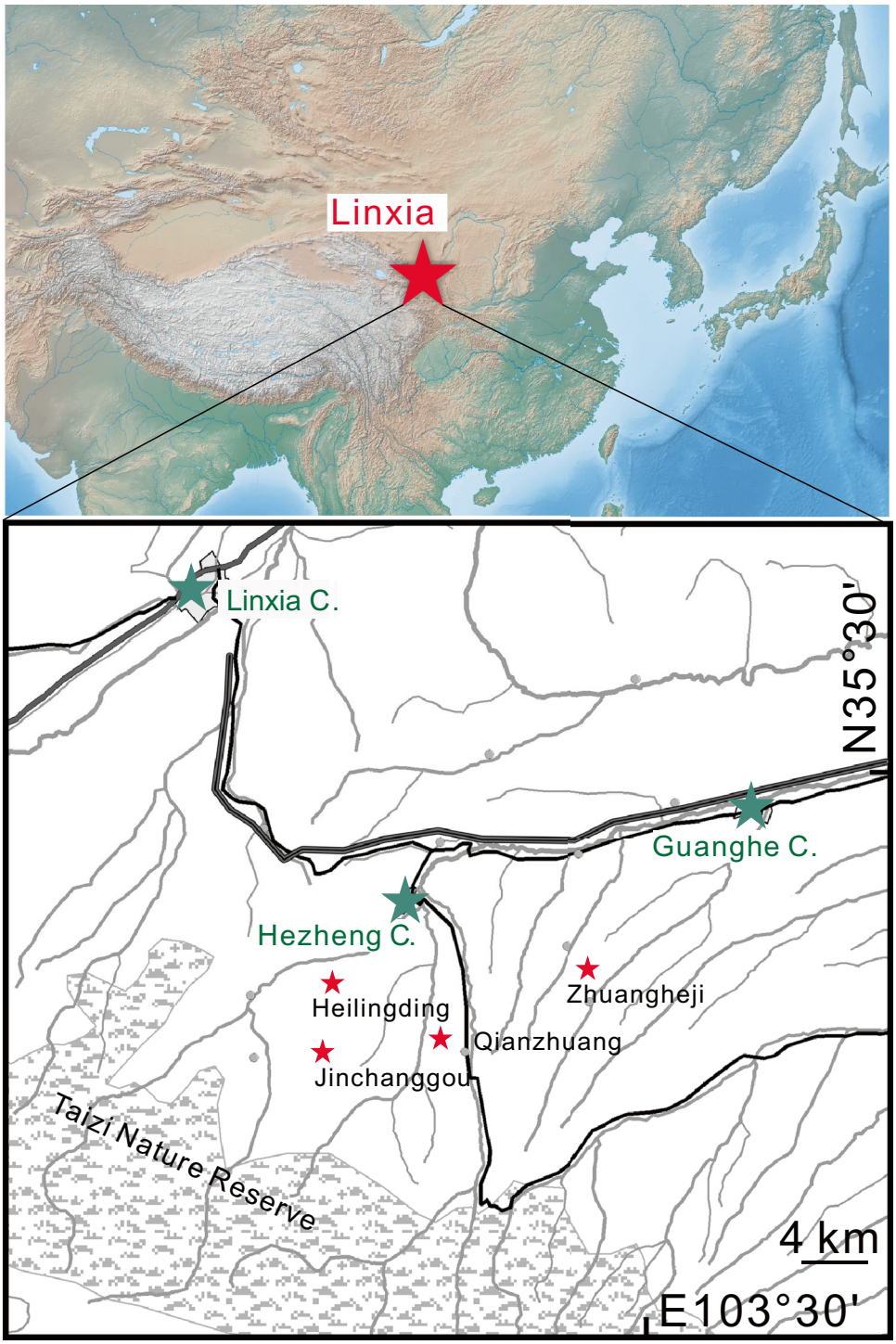

Fig. 1 Localities bearing *Pliorhinus ringstroemi* from the Linxia Basin. The large green stars represent the centers of the counties, and the small red stars represent fossil localities producing *Pliorhinus ringstroemi*. The black lines present road, and light gray lines represents rivers

phylogeny published by Liu et al. (2021) as a topological constraint as (*Rhinoceros unicornis*, *Rhinoceros sondaicus*), (*Dicerorhinus sumatrensis*, (*Coelodonta antiquitatis*, *Stephanorhinus kirchbergensis*))). We adopt this constraint as large dataset of DNA is less prone to convergent evolution and is more likely closer to true phylogenetic relationship than that inferred from morphology. We also perform the maximum parsimony analysis using the software TNT 1.6 (Giribet 2005; Goloboff and Catalano 2016). This analysis finds the tree with shortest length, which is assumed to most likely reflect the evolutionary history based on the criterion of parsimony. This is an alternative method to find out the most well-supported phylogenetic tree for comparison with the Bayesian inference method. The traditional search with the TBR swapping algorithm was used, with 1,000 replications, and the results (see Online Resource 6) are generally

Table 1 Measurements (in mm) of *Pliorhinus ringstroemi* skulls (indicated by specimen numbers) compared with samples of *P. megarhinus*, *Dih. pikermiensis* and *Dih. schleiermacheri* from (Pandolfi et al. 2015)

	HMV1115	HMV1343	HMV1419	HMV1418	HMV2048	HMV2049	*P. megarhinus*	*Dih. pikermiensis*	*Dih. schleiermacheri*
Locality	Qianzhuang	Jinchanggou	Zhuangheji	Zhuangheji	Heilingding				
Distance between nasal tip and occipital	713	738	>731	699	679.02	430	700-787.5	615-660	654-667
Distance between nasal notch and orbit	124.92	144.88	118.14		135.22	77.03			
Length of P2-M3	272.89	256.09	263.95	253.56	318.94		255-280	240-272	267

similar. We believe that the tip-dating Bayesian analysis, which uses chronological data, is more likely to reflect the true phylogeny, so our interpretation is mainly based on the tip-dating tree.

Systematic paleontology

Order Perissodactyla Owen, 1848.
Superfamily Rhinocerotoidea Gray, 1821.
Family Rhinocerotidae Gray, 1821.
Subfamily Rhinocerotinae Gray, 1821.
Tribe Rhinocerotini Gray, 1821.
Genus ***Pliorhinus*** Pandolfi et al., 2021.

Type species: *Pliorhinus megarhinus* (de Christol, 1834).
Included species: *Pliorhinus miguelcrusafonti* (Guérin & Santafé-Llopis, 1978), *Pliorhinus ringstroemi* (Arambourg, 1959).
Emended diagnosis (modified from Pandolfi et al. 2021): Medium- to large-sized two-horned Rhinocerotina with foramen infraorbital and nasal notch located above the P4-M1, high zygomatic arch, occipital face backward inclined, developed nuchal tubercle, sub-triangular foramen magnum, P1 usually absent in adults, transverse metaloph on P2, protoloph always interrupted on P2, crista always present on P3, posterior part of the ectoloph concave on M1 and M2, constriction of the protocone usually absent on M3, angular trigonid on the lower teeth, obtuse or right dihedron trigonid on the lower teeth, the smooth anterior side of the semilunate, mediolaterally symmetric distal facet for the semilunar on the pyramidal, and curved magnum facet on McII.

Pliorhinus ringstroemi (Arambourg, 1959).
Selected synonymy:
Dicerorhinus orientalis: Ringström 1924: p. 5; Ringström 1927: p. 14; Teilhard de Chardin and Leroy 1942: p. 64; Liu et al. 1978: p. 176; Zhang et al. 1978: p. 22; Yuan and Du 1984: p. 109; Qiu and Qiu 1990: p. 64.

Table 2 Measurements (in mm) of the mandible of *Pliorhinus ringstroemi* from Heilingding (HMV2048)

	Left	Right
Length	579.14	565.18
Height of horizontal ramus in front of p2	66.41	
Height of horizontal ramus in front of p3	104.25	102.81
Height of horizontal ramus behind m3	114.43	115.46
Height at condyle	232.4	
Height at coronoid process	296.87	
Length of p2-m3	324.64	333.06
Length of p2-p4	132.06	132
Length of m1-m3	190.36	198.54

Table 3 Measurements (in mm) of the upper teeth of *Pliorhinus ringstroemi*

	HMV1115	HMV1343	HMV2049
Locality	Qianzhuang	Jinchanggou	(unknown)
DP1 Length			35.43
DP1 Width			24.13
DP2 Length			43.04
DP2 Width			35.97
DP3 Length			45.36
DP3 Width			44
DP4 Length			51.76
DP4 Width			50.23
P2 Length	39.55	36.47	
P2 Width	49.2		
P3 Length	45.27	38.98	
P3 Width	61.62	54.66	
P4 Length	46.8		
P4 Width	68.05		
M1 Length	52.5	45.78	
M1 Width	72.3	69.69	
M2 Length	63.28	47.53	
M2 Width	73.96	72.46	
M3 Length	66.17	75.15	
M3 Width	65.97	66.18	

Dicerorhinus orientalis var. *ringströmi*: Arambourg, 1959, p. 73.
Dicerorhinus ringstroemi: Chen and Wu 1976, p. 9; Yan 1978, p. 31.
Dicerorhinus ringstromi: Tong et al. 1979, p. 495; Deng and Wang 2004, p. 222; Deng 2006, p. 51.
Dicerorhinus ringströmi: Yuan and Du 1984, p. 132.
Stephanorhinus Orientalis: Zhang et al. 2002, p. 170.
Dihophus Ringstroemi: Deng et al. 2011, p. 1287; Tong 2012, p. 556.
"*Dihoplus*" *megarhinus* : Pandolfi et al. 2015, p. 327; Pandolfi and Rook 2017, p. 47.
Pliorhinus megarhinus : Pandolfi et al. 2021, p. 4; Pandolfi et al. 2022, p. 4.

Lectotype: PMU M448, skull from Shangyingou, Xin'an, Henan Province, central China.

Geographic and chronological distribution: Baode, Xin'an, and Linxia Basin, central to northern China, Baodean (equivalent to MN12 of Europe, the Late Miocene).

Emended diagnosis: Large-sized two-horned rhinoceros, skull dolichocephalic, nasal septum not ossified, nasal bone elongated and wide, with strong doomed horn boss, nasal notch reaching P4, anterior border of orbit at middle M2; Preorbital tubercle and lacrimal tubercle strong, postorbital process weak; Dorsal profile concave, fused posttympanic and the postglenoid processes, false exterior auditory meatus; Mandible ascending ramus vertical, symphysis upraised; I1 large and oval, I2 absent; di1 small and round, i2 tusk-like; DP1 small and lost in adult, Upper cheek teeth labial cingulum usually absent, lingual cingulum weak and reduced, paracone fold strong; Upper premolars protocone not constricted, antecrochet absent; Lower cheek teeth labial and lingual cingulum usually absent.

Differential diagnosis: *Pliorhinus ringstroemi* differs from the genus *Diceros* in having a larger size, longer and thinner nasal bone, lower cranium, and less elevated occipital part. *P. ringstroemi* differs from *Miodiceros neumayri* in having longer and thinner nasal bone, more complex upper cheek teeth, and taller and vertical ascending ramus in manidble. *P. ringstroemi* differs from *Dicerorhinus* in having bigger nasal bone, deeper nasal notch, and premolar that protocone and hypocone fused. *P. ringstroemi* differs from *Dihoplus schleiermacheri* in having shorter premaxilla, smaller I1, and absence of the I2. *P. ringstroemi* differs from *Dihoplus pikermiensis*, in having a longer nasal and deeper nasal notch, bigger I1, and vertical ascending branch. *P. ringstroemi* differs from *P. megarhinus* in having developed and oval I1, and tusk-like i2. *P. ringstroemi* differs from *P. miguelcrusafonti* in having more anterior foramen infraorbital, upper premolars with a lingual bridge between protocone and hypocone, and nearly vertical ascending ramus.

Description A total of five adult or subadult skulls and one juvenile skull were found in the Linxia Basin. Unfortunately, most of them are either slightly to moderately deformed or incomplete. Our description is mainly based on the most complete skull HMV1419, supplemented by other specimens. The skull HMV1419 is complete, especially having the premaxillae preserved, which is important for clarifying its taxonomical status. The teeth are deeply worn, indicating the specimen represents an old individual. The description of cheek teeth below is mainly be based on the young adult skull HMV2048, supplemented by other specimens. The deciduous teeth are described based on the juvenile individual HMV2049.

Skull The skull (Fig. 2) is dolichocephalic. It is relatively low in HMV1418 and HMV1419, but this is likely a result of dorso-ventral compression, and in two undeformed skulls, the skull is rather high. The dorsal profile of the skull is concave, rising in its posterior third. The nasal septum is not ossified, and the nasal bone is elongated and wide, with a horn boss. The nasal notch usually reaches the level of P4 but only reaches the level of P3 in the young adult HMV2048. The nasal notch is V-shaped in HMV1419, but this is probably due to dorso-ventral compression, and in the two undeformed skulls it is U-shaped. The nasal is nearly straight in HMV1343 but strongly curved in HMV1115 and HMV2048. The area with rough vascular rugosity on the surface of the nasal is large and distinct, indicating a large nasal horn. The nasal bones are fused, but there is a shallow median groove from the tip of the nasals until the top of the horn dome.

The infraorbital foramen is open at the level of P3/P4, exactly the same as the posterior border of the nasal notch. The anterior border of the orbit is above the middle of M2. The lacrimal and preorbital processes are both present and distinct. The postorbital processes of the frontal and jugal are both very weak and indistinct. The base of the zygomatic process on the maxilla is high: it begins several centimeters above the M2. The zygomatic arch is moderately deep and its anterior part is inclined medially (dorsal side in medial position). The forehead is wide and flat. The area with rough vascular rugosity on the surface of the frontal is present and strongly developed in old individuals such as HMV1419, and is slightly smaller in HMV1418, smaller and less distinct in younger individuals HMV2048. There is a distinct separation between the fronto-parietal crests from both sides, in HMV1419 and most other individuals, but in one specimen HMV1418, the two crests unite into a sagittal crest. The case in this specimen probably represents a rare variant of this species, as most other traits of HMV1418 are

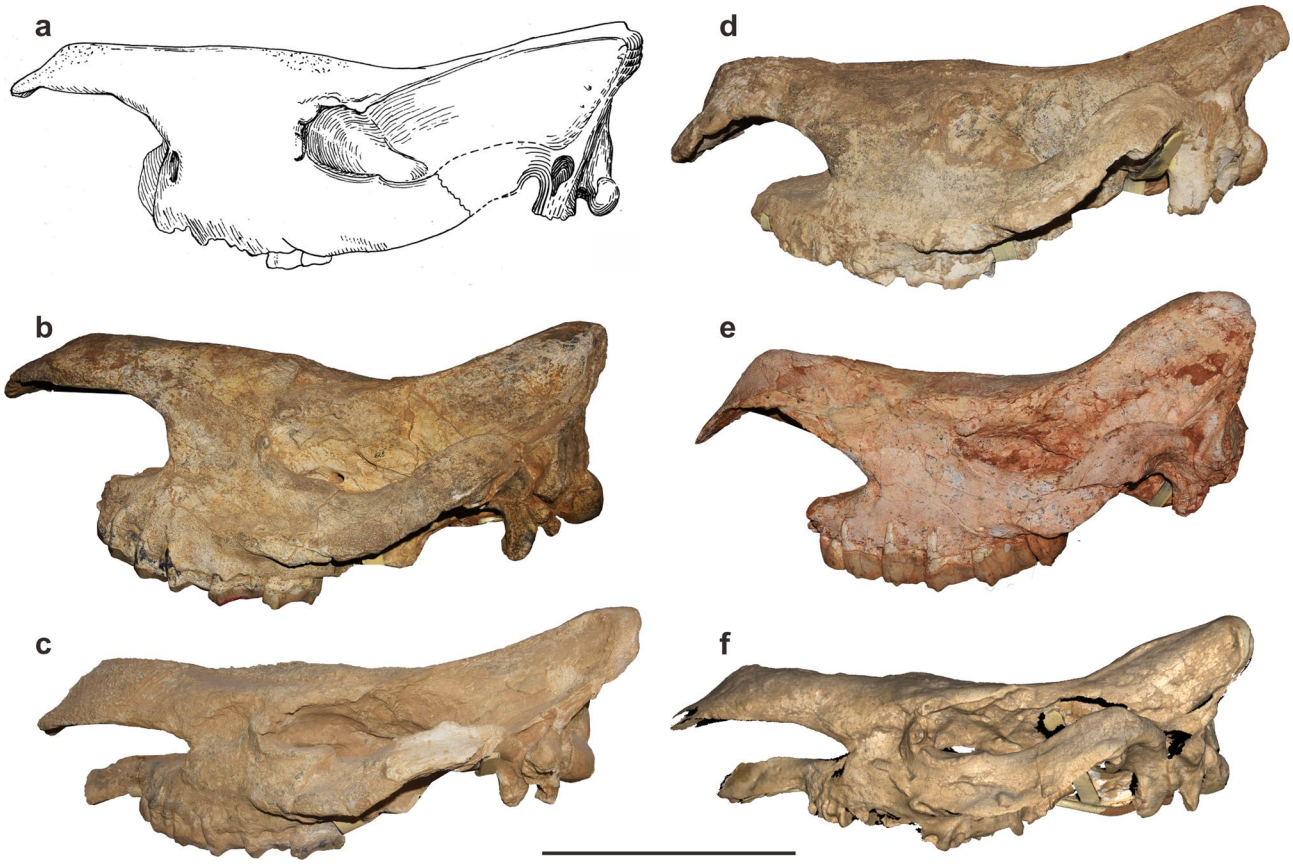

Fig. 2 *Pliorhinus ringstroemi* crania in left lateral view. **a**. M448 (reversed), Shangyingou, Xin'an (Ringström 1924); **b**. HMV1115, Qianzhuang; **c**. HMV1419 (reversed), Zhuangheji; **d**. HMV1343, Jinchanggou; **e**. HMV2048 (reversed), Heilingding; **f**. HMV1418, Zhuangheji. Scale bar equals 30 cm

indistinguishable from other specimens. The occipital crest (dorsal view) is smoothly concave in HMV1419 and most other specimens, but in HMV1418 it is strongly concave and nearly forked. The occipital plane is inclined backward but only slightly, as the occipital condyle is only slightly anterior to the occipital crest in undeformed skulls.

The premaxilla is thin, elongated (not reaching the level of the nasal tip), and extends slightly ventrally. The premaxillae from both sides are not attached to each other. The distance between the anterior border of the premaxilla to the anterior base of the P2 alveolus is around 127 mm in HMV1419, and this value is 159 mm in another specimen (HMV1418) preserving the premaxilla. The cheek toothrows from both sides diverge backward. The width between the toothrows from both sides is slightly wider in its middle and distal parts than in its anterior part. The anterior border of the bony choana reaches the level of the M2. The posterior margin of the pterygoid is nearly horizontal. The postglenoid process is rodlike and straight, and its cross section is convex. The external auditory pseudomeatus is closed by the postglenoid process and posttympanic process. The posttympanic process is strongly developed and laterally expanded. The paroccipital process is distinct and extends ventrally to the same extent as that of the postglenoid process. It is thinner than the postglenoid process and has a concave anterior surface. The foramen magnum is sub-triangular. There is no median transverse ridge in the occipital condyle (Fig. 3).

The only subadult mandible is from HMV2048 (Fig. 4). The horizontal corpus is moderate in depth. Its anterior part is markedly shallower than the main body, causing a convex ventral profile of the mandible. The symphysis is narrow, not wider than the distances between the p2s. The posterior border of the symphysis reaches the level of p3. The mental foramen is present below p2. The ascending ramus is massive. Its anterior border is nearly perpendicular to the toothrow. The mandibular condyle is slightly transversely convex. The coronoid process is small, with a hook-like posterior border.

The juvenile skull (Fig. 5) has DP1-4 preserved, and the DP4 is not fully erupted, suggesting an age of around 1.5 years using the criterion of *Ceratotherium* (Hillman Smith, 1986). The nasal is already rather elongated and wide, with a smooth surface. The nasal notch is U-shaped. Its posterior

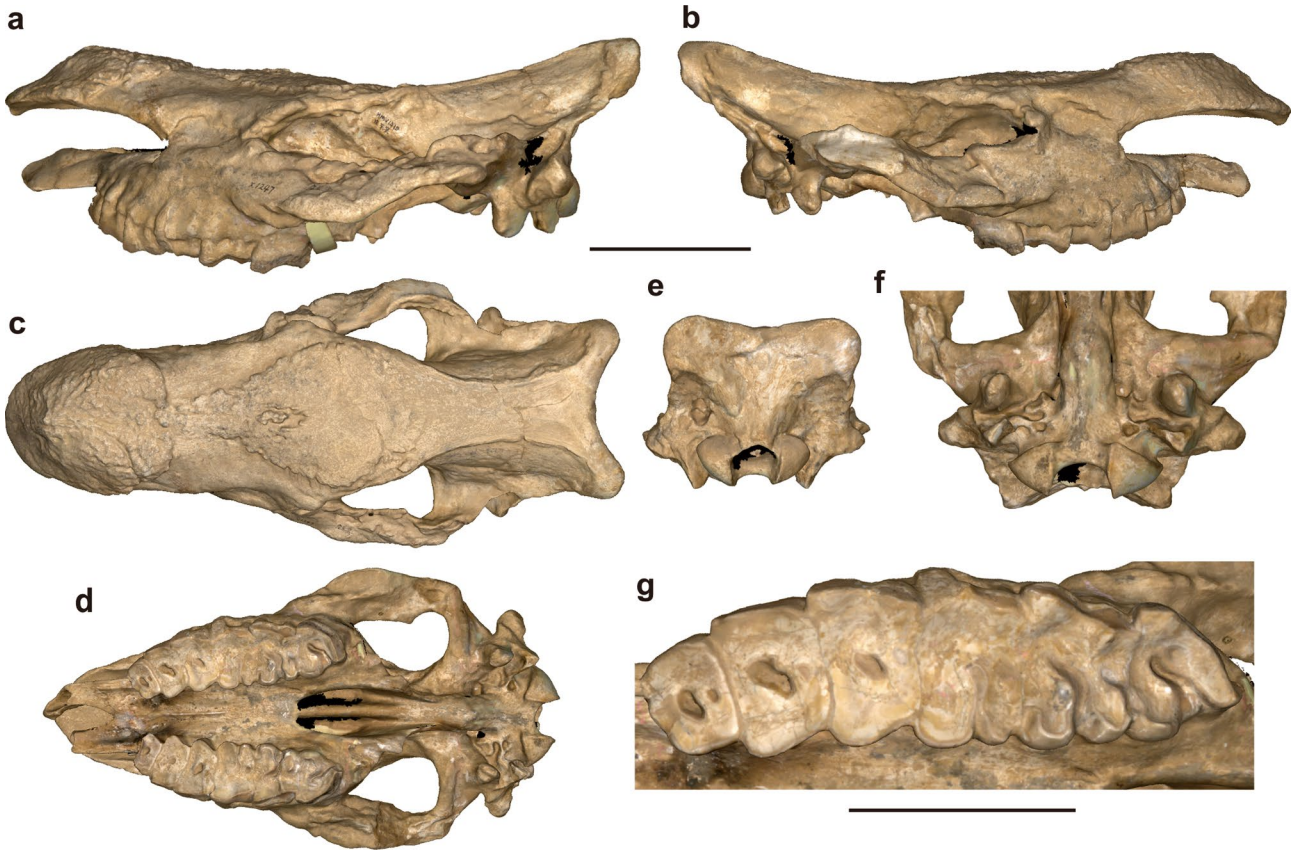

Fig. 3 Cranium of *Pliorhinus ringstroemi* (HMV1419). **a**. left lateral view; **b**. right lateral view; **c**. dorsal view; **d**. ventral view; **e**. caudal view; **f**. enlarged view of ventral basicranial region; **g**. Left P2-M3, occlusal view. Scale bar equals 20 cm in **a-f** and 10 cm in **g**

border lies at the level of the DP2, and the infraorbital foramen also lies at this level. The lacrimal and preorbital processes that are well-developed in adults are absent. The dorsal profile is concave as in adults. The external auditory pseudo-meatus is already closed by the postglenoid process and posttympanic process. The postglenoid process is thinner than that of the adults. The posttympanic process is less expanded compared with that in adults. The premaxilla is short, with a thin anterior end, and lacks the trace of development of the incisor. The zygomatic arch is less inclined than in the adult. The mandible is shallower than in adults, and the anterior border of the ascending ramus is more backward inclined.

Upper teeth The I1 is developed, and I2 is absent. The I1s in HMV1418 are large, oval in shape, and deeply worn with a diameter of 28.26*13.92/28.06*15.71 mm. HMV1419 preserves the alveolus of I1 which measure 37.05*18.55 mm.

The upper cheek teeth (Fig. 6) have weak cement on the labial side. The postfossette is deep and narrow. The secondary folds are usually complex. The labial cingulum is absent in P4 and molars, but a reduced lingual cingulum is present in P2 and P3. In the upper premolars, the protocone is not constricted and forms a lingual bridge with the hypocone. The antecrochet is absent, and the crochet is narrow. The crista is multiple. The parastyle and paracone ribs are weak in P2 but developed in P3 and P4. The protoloph is thin but continuous and connected with the ectoloph in P2, and becomes stronger in P3 and P4. In the upper molars, the protocone is distinctly constricted. The hypocone is weakly constricted. The parastyle is wide and projected. The antecrochet is short, and the crochet is well-developed. The M1 and M2 have marked paracone ribs, and M3 has a triangular occlusal surface. The metastyle is long and the posterior part of the ectoloph of M1 and M2 is concave.

In the deciduous upper cheek teeth, the lingual cingulum is absent. The protocone is separated from the hypocone in slight wear stages. The crochet is narrow, occasionally multiple. The antecrochet and crista are usually absent. DP1 is double–rooted with a roughly triangular outline. The parastyle is long and the DP1 is longer than wide. In DP2-4, the outline is roughly square. The median valley is deep, and the posterior fossette is V–shaped. The protoloph and the metaloph are backwardly inclined. The parastyle is developed but

Fig. 4 Mandible of *Pliorhinus ringstroemi* (HMV2048). **a**. dorsal view; **b**. left lateral view. Scale bar equals 20 cm

weaker successively from DP2 to DP4. The mesoloph and mesostyle rib are only well developed in DP2, but very weak in DP3 and absent in DP4. The paracone rib is well developed in DP3 and DP4. The constriction on the hypocone is present in DP2-4, and the constriction on the protocone is present in DP3 and DP4.

Lower teeth A pair of di1 can be observed, they are small and round, and have a little distance between each other, with a diameter of 5.32*5.23 mm. The i2s are tusk-like, nearly parallel, and have been distinctly worn in the young adult HMV2048, with a diameter of 18.81*15.77 mm. In the juvenile mandible HMV2049, only the left di1 is preserved, and no evidence proves the presence of di2 and di3.

In the lower teeth, the labial cingulum is absent. The lingual cingulum is very reduced in premolars, and absent in molars. The external groove is present and reaches the base of the crown. The crown is higher in premolars than in molars. The posterior valley is shallow, and its lingual opening is V-shaped. The p1 is absent. The p2 has isolated paralophid and reduced paraconid. The hypolophid in the lower molars is oblique.

In the deciduous lower cheek teeth, the cingulum is absent. The dp1 has only one lobe, its valley is shallow and closed. The posterior valley of dp2 is also closed before being worn. The paralophid is double in dp2 and dp3 but simple, as the dp3 is longer than dp4. The posterior valley is open in dp3 and dp4 with a V-shaped lingual opening.

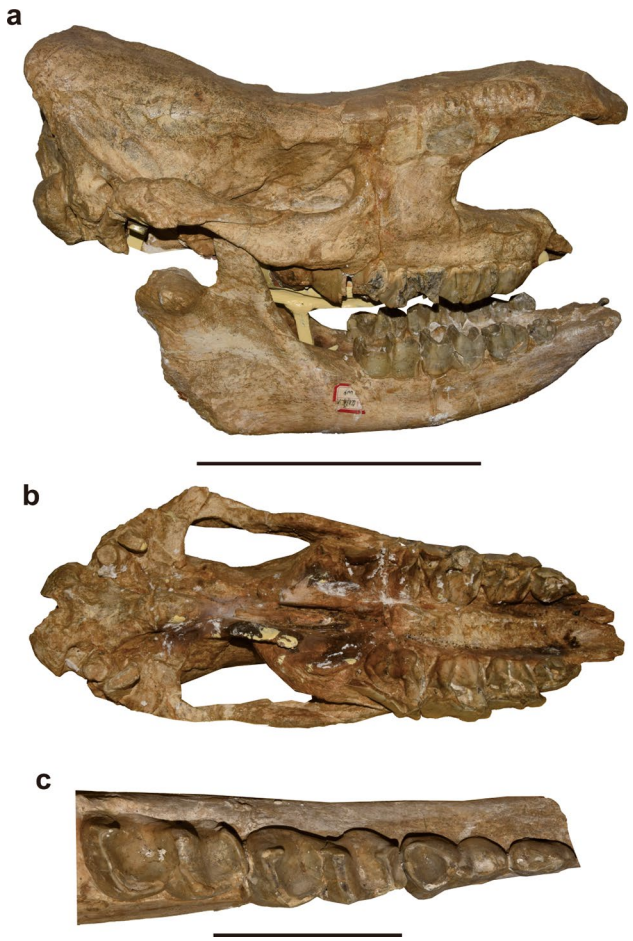

Fig. 5 Juvenile cranium and mandible of *Pliorhinus ringstroemi* (HMV2049). **a**. right view; **b**. skull, ventral view; **c**. dp1-dp4, occlusal view. Scale bar equals 20 cm in **a-b** and 5 cm in **c**

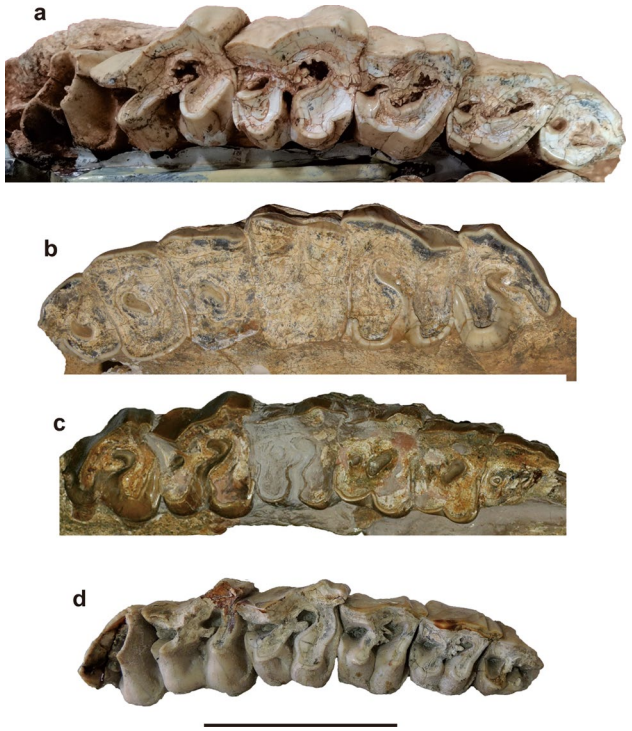

Fig. 6 Comparison of *Pliorhinus* upper teeth. **a**-**b**. *Pliorhinus ringstroemi* **a**. HMV2048, right P2-M3; **b**. HMV1115, left P2-M3; **c**. *Pliorhinus megarhinus* from Baccinello (NMB BAC n.c, right P2-M3; image from Pandolfi and Rook 2017); **d**. *Pliorhinus miguelcrusafonti* from Kvabebi (GNM1 29-2013/925 DN-229, right P2-M3; image from Pandolfi et al. 2021). Scale bar equals 10 cm

Comparisons

The new materials described in this study are clearly different from Dicerotini in having a larger but thinner nasal, shallower nasal notch. They further differ from *Diceros gansuensis* in having a larger size, lower cranium, thinner zygomatic arch, and less elevated occipital part. They further differ from *Miodiceros neumayri* in having longer and thinner nasal bone, taller and vertical ascending branch, and premolars that have fused protocone and hypocone.

Our material is generally similar to *Dihoplus*, but it differs from *Dihoplus schleiermacheri* in having smaller I1, and the absence of the I2. They are different from *Dihoplus pikermiensis*, in having longer nasal and deeper nasal notch, and the external auditory pseudo-meatus fully closed (Geraads 1988; Giaourtsakis 2022). Therefore, our materials should be assigned to *Pliorhinus*. The skull of *P. ringstroemi* is bigger than the skulls of *Dih. Schleiermacheri* and *Dih. Pikermiensis*, and on average smaller than the skulls of *P. megarhinus*.

Deng (2006) first studied the two-horned rhinoceroses in Linxia Basin and identified them as *Dicerorhinus ringstromi* (=*Pliorhinus ringstroemi*). The skulls studied here share the following characters with the type specimen: dolichocephalic skull, concave skull roof, huge nasal horn boss, nasal notch ends at the level of the P3/P4 boundary, strong preorbital tubercle and well-developed lacrimal tubercle, triangular occipital condyles, fused posttympanic and postglenoid processes, convex ventral profile of horizontal corpus, upraised the tip of the symphysis, mental foramen below p2. HMV1115 is the one with the closest morphology to the type specimen from Xin'an. Except for the slight variation in position and shape of the nasal notch, the new specimens described are similar to HMV1115 and the type. These differences will be further discussed in the intraspecific variation section.

Pandolfi et al. (2015) compared *P. megarhinus* and *P. ringstroemi* in detail, and considered *P. ringstroemi* as a junior synonym of *P. megarhinus* based on the following shared characters: distant frontal-parietal crests, closed external auditory pseudomeatus, absence of I2 and i1, reduced i2; Paracone fold weak on upper premolars, and marked on upper molars; Small crista on M3. After we

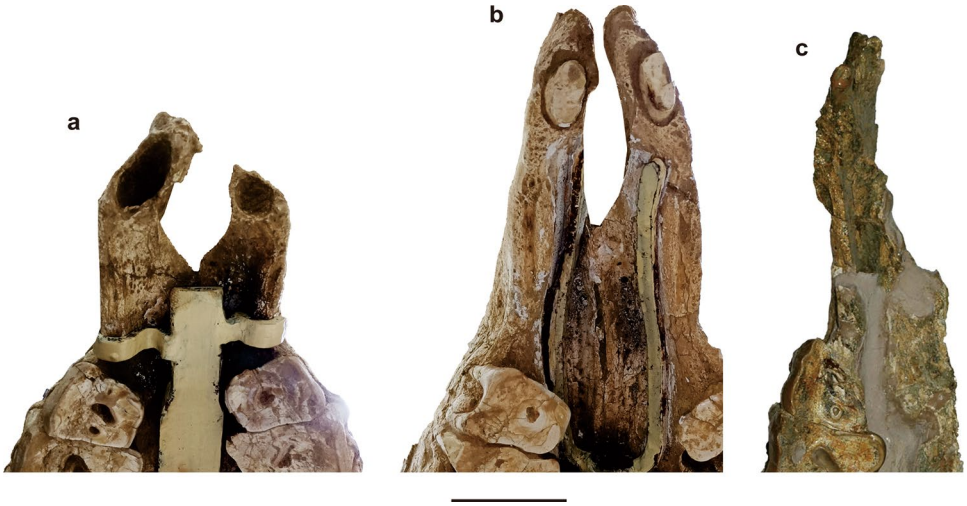

Fig. 7 Comparison of the premaxillae of *Pliorhinus* in ventral view. **a**-**b**. *Pliorhinus ringstroemi*. **a**. HMV1419; **b**. HMV1418; **c**. *Pliorhinus megarhinus* (NMB BAC n.c., from Pandolfi and Rook 2017). Scale bar equals 5 cm

observed new specimens, most of these shared characters are still valid, except for the strong paracone fold on upper premolars with little wear in HMV2048. Pandolfi et al. (2015) described the I1 of *P. megarhinus* as "small and rounded", and the right upper maxilla with I1 of *P. megarhinus* was present from Pandolfi and Rook (2017). The new specimens from Linxia provide some new characters, especially about the premaxilla and incisors. The I1 of *P. ringstroemi* is developed and oval (Fig. 7), and i2 is tusk-like and functional (with clear wear facet), both relatively larger and more pronounced than those of *P. megarhinus* (Pandolfi 2013). Compared to the type specimen of *P. megarhinus* (MNHN AC2683), the secondary folds in *P. ringstroemi* on upper cheek teeth are more complex. The base of the corpus of the mandible is more convex. The ascending ramus of *P. ringstroemi* is nearly vertical (can be seen more clearly in the scan model on https://figshare.com with the doi: 10.6084/m9.figshare.23896449), whereas that of *P. megarhinus* is inclined backward (Guérin 1980). The mandibular foramen of *P. ringstroemi* is higher than that of *P. megarhinus*, above the teeth-neck level.

The *P. miguelcrusafonti* materials published are poorly preserved. *P. ringstroemi* can be separated from *P. miguelcrusafonti* based on more anterior foramen infraorbital, upper premolars have a lingual bridge between protocone and hypocone, and nearly vertical ascending ramus.

The specimens from Linxia show some notable intraspecific variations previously unknown in *P. ringstroemi*, including the level of development of nasal and frontal horn bosses, the shape of the nasal bone and nasal notch, the width of the frontoparietal crest, and the shape of the occipital crest. In the five known adult skulls (M448, HMV1115, HMV1343, HMV1418, HMV1419), the nasal and frontal horn bosses of HMV1343 and HMV1419 are extremely developed and protruding from the surface of the bone, others are less developed, and the rough surface of the young adult skull (HMV2048) is barely visible. This difference may be related to gender (in the living white rhino, horns are more developed in males; (Owen-Smith 1988)). The premaxilla of HMV1419 is significantly shorter than that of HMV1418, the I1 is also somewhat smaller (Fig. 8). The anterior part of the nasal bone is

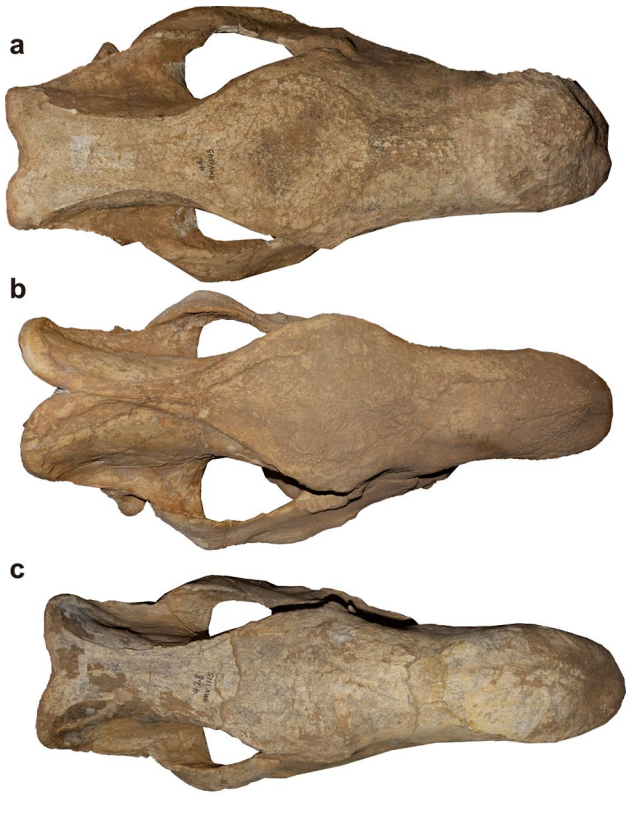

Fig. 8 Dorsal view of the skull of *Pliorhinus ringstroemi*. **a**. HMV1343; **b**. HMV1418; **c**. HMV1419. Scale bar equals 30 cm

slanted downward, it is weak in M448 and HMV1115, moderate in HMV1418 and HMV1419, and strong in HMV1343 and HMV2048. In HMV1343, the developed nasal horn boss thickens the nasal bone, making it more curved with an obvious dorsal convexity, but in HMV2048 it has a similar nasal bone convexity without rough vascular rugosity, showing that the curved nasal bone is not relevant to ontogenetic. The posterior part of HMV1418 is unusual, the frontal-parietal crest is fused in a sagittal crest, and the occipital crest is forked. The compression occurred in the dorso-ventral direction, and do not influence the occipital crest. In others (including HMV1419 which has nearly the same compression as HMV1418) the surface between the parietal crests is wide and the occipital crest is concave. These two characters are frequently used in phylogenetic matrices, but in *P. ringstroemi* they show a great variation. The width of frontal-parietal crest also varies in living rhinos. The studies of tapirs show that sagittal crest development level is poorly correlated with relative cranial bite force, and this character might be not functionally related (Abernethy 2011; Linden et al. 2022).

Geometric morphometric analyses

Figure 9 plots PC1 (X axis) (41.02% of the total shape variance) and PC2 (Y axis) (22.13% of the total shape variance) of the lateral view. Negative PC1 values are associated with a cranium showing uplifted nasals and forward-inclined occipital surface. Living *Rhinoceros* is clearly separated from others with the lowest score. Positive PC1 values are associated with a cranium with a flat nasal and backward-inclined occipital surface like *Ceratotherium simum* and some *Coelodonta*. Negative PC2 values are associated with a long and thin nasal bone and a long posterior part of the cranium, as in some *Stephanorhinus* and *Coelodonta*. Positive PC2 values are associated with a short and thick nasal bone, short nasal notch, high posterior side of cranial, and concave dorsal profile. This morphology is most pronounced in *Diceros bicornis*.

P. ringstroemi is located in the central part of the morphospace. The PC1 scores of *P. ringstroemi* and *P. megarhinus* are close to zero, implying their occipital plane is relatively vertical. The PC2 scores of *P. ringstroemi* are low

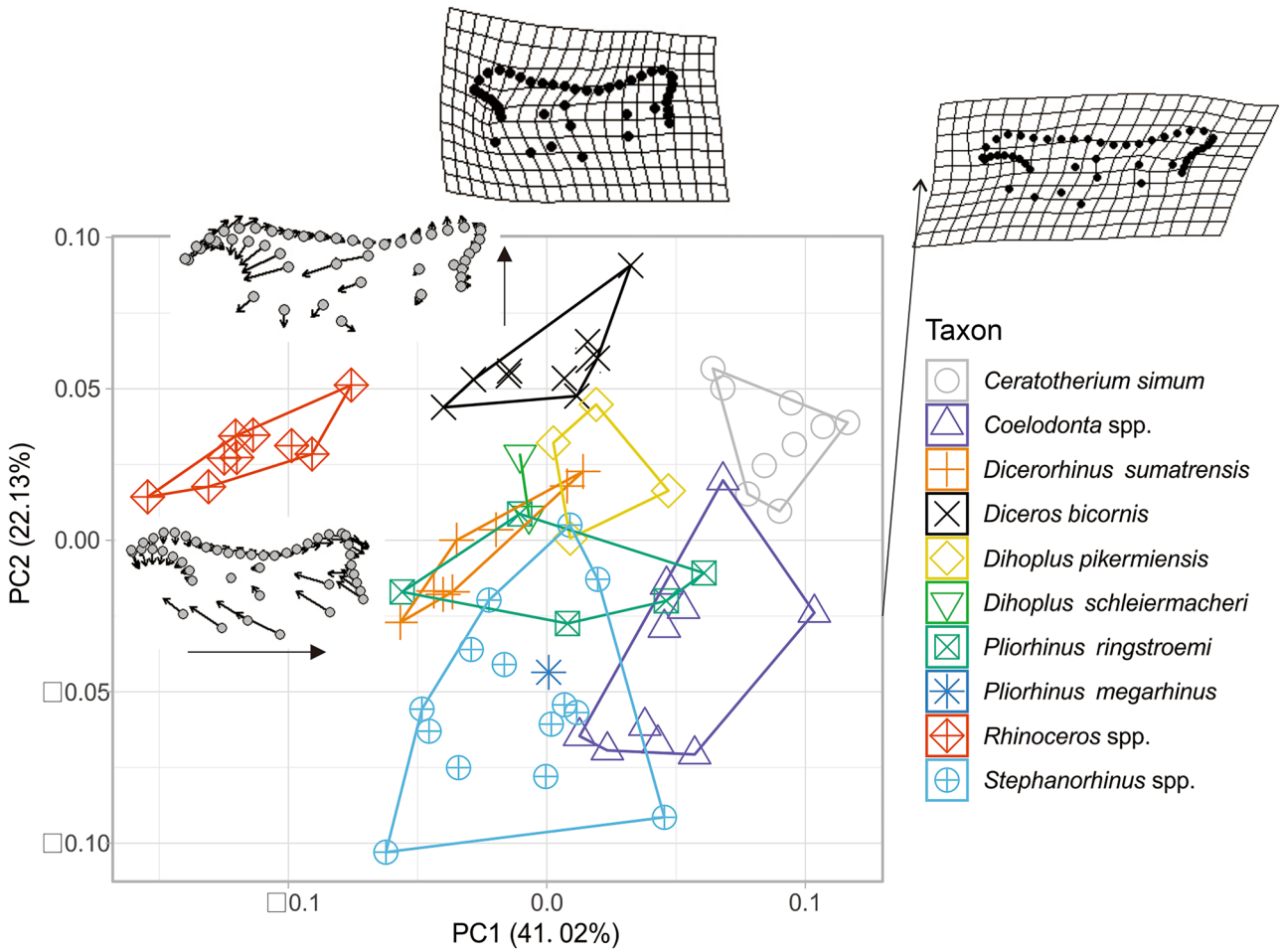

Fig. 9 GM plot of lateral view of the cranium of *Pliorhinus* and related taxa

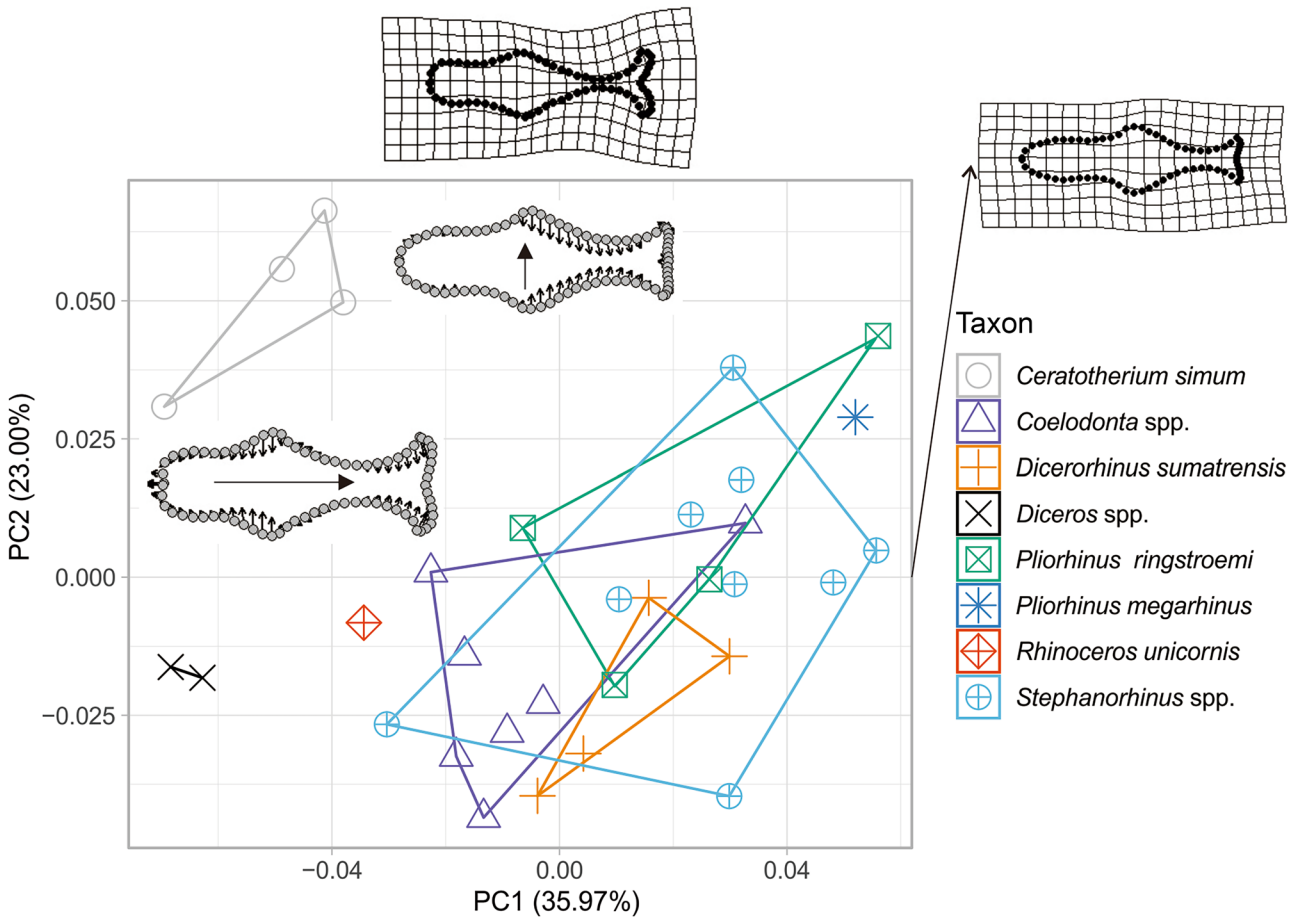

Fig. 10 GM plot of dorsal view of the cranium of *Pliorhinus* and related taxa

and still lower in *P. megarhinus*, which suggests a long nasal and low cranium. *Stephanorhinus* has the lowest PC2 scores, which distinguishes it from other genera rhinos.

Figure 10 plots PC1 (35.97% of the total shape variance) and PC2 (23.00% of the total shape variance) of the dorsal view. Negative PC1 values are associated with short and wide nasal bone, wide frontal, and long occipital crest. *Diceros bicornis* and *C. simum* show the lowest score on it. Positive PC1 values are associated with long and thin nasal, thin frontal, and short occipital crest. Negative PC2 values are associated with a wide frontal-parietal crest and flat occipital crest. Positive PC2 values are associated with fused sagittal crest and forked occipital crest, like *C. simum*. The unique individual HMV1418 with a sagittal crest and nearly forked occipital crest shows a much higher PC1 and PC2 score than other *P. ringstroemi*, some *Stephanorhinus* and *P. megarhinus* also have high scores. Most species cannot be distinguished from each other. *P. ringstroemi* is partially overlapped with *Stephanorhinus*, *Dic. sumatrensis*, and *Coelodonta*.

In summary, the morphospace occupied by *P. ringstroemi* is different from that of the type of *P. megarhinus*. There is a continuous variation between *Dihoplus*, *P. ringstroemi* and *P. megarhinus* in lateral view, and less clearly in dorsal view.

Phylogenetic analysis

Our phylogeny (Fig. 11) suggests that *P. ringstroemi* forms the sister group of the younger species of *Pliorhinus*, i.e., *P. megarhinus* and *P. miguelcrusafonti* with high posterior probability. Autapomorphies of *P. ringstroemi* include: processus zygomaticus maxillary brutal, transversal profile of the articular tubercle concave, processus posttympanicus well-developed, processus coronoideus little-developed, foramen mandibulare above teeth-neck level, i2 shape tusk-like, upper molars antecrochet usually present, M1-2 metacone fold present, M3 posterior groove on the ectometaloph present, D3-4 mesostyle absent, d2 posterior valley usually closed. Synapomorphies of the *Pliorhinus* include: zygomatic/frontal widths equal or more than 1.5, processus postglenoidalis (articulation, in cross section) convex, sagittal crest on the basilar process absent, upper molars crista usually present, M1-2 posterior part of the ectoloph concave, M1-2 posterior cingulum low and interrupted, d2 posterior valley usually open.

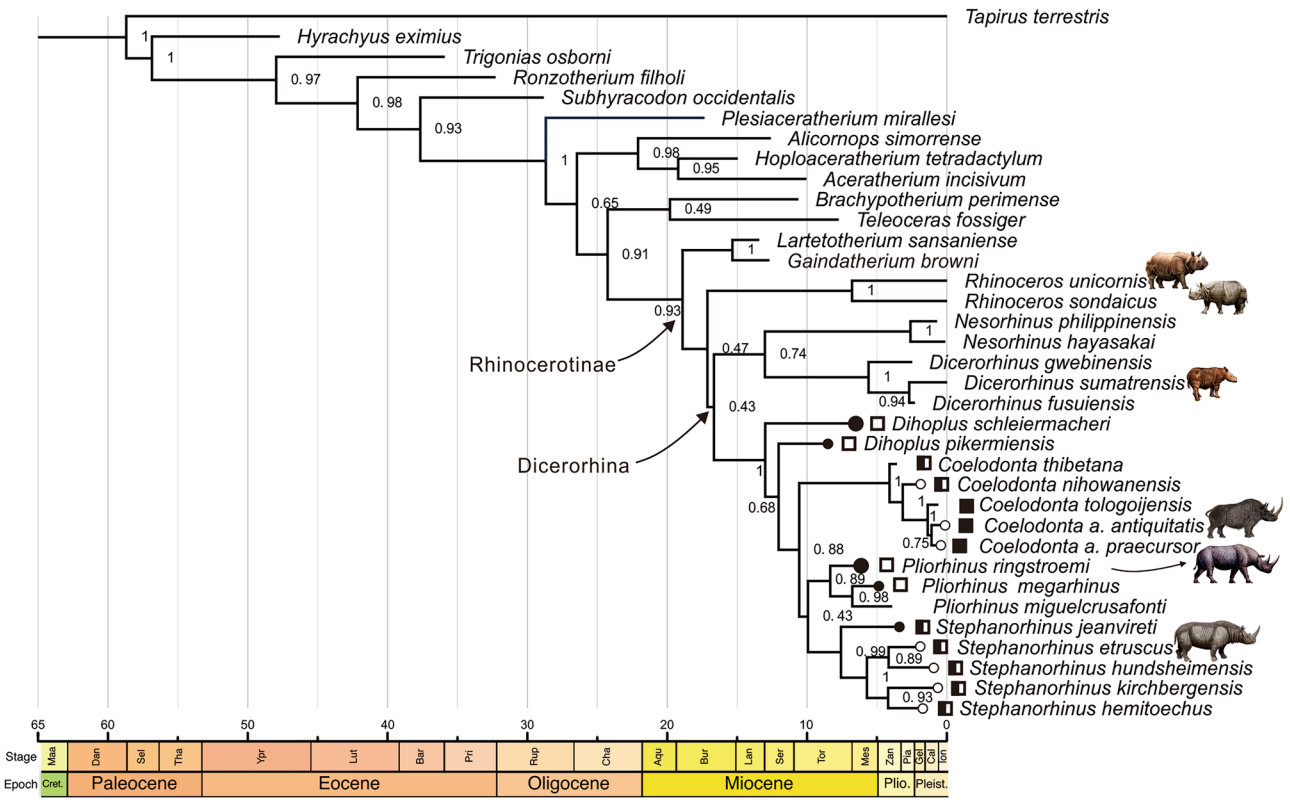

Fig. 11 Phylogeny inferred from Bayes Inferences, with the node support marked in nodes. The numbers in nodes represent posterior probabilities. In the Dicerorhina branch, the large black circle means that I1 is large, the small black circle means that I1 is small, the hollow circle means that I1 is absent, and the lack of any circle means that I1 is not known; the black square means that nasal septum is totally ossified, the half black and half white square means that nasal septum is partly ossified, the hollow square means that nasal septum is never ossified, and lack of any square means that nasal septum is not known (not preserved in any specimen of this species). The reconstructions are from Binia De Cahsan and Yu Chen

As *P. ringstroemi* appeared earlier in Eastern Asia, and then other species appeared in Europe, *Pliorhinus* most likely originated in eastern Asia and spread to Europe. In our phylogeny, *Pliorhinus* forms a sister group to *Stephanorhinus*, but this node only has a very low posterior probability. This suggests that the relationship between *Pliorhinus*, *Stephanorhinus*, and *Coelodonta* is not fully clear. *Dihoplus* is basal to the monophyly of *Pliorhinus*, *Stephanorhinus*, and *Coelodonta*, and *Dicerorhinus* is an earlier divergent branch. The result of maximum parsimony analysis by TNT shows a similar result (see Online Resource 6) with a same relationship between *Pliorhinus*, *Stephanorhinus*, and *Coelodonta*, but some branches such as *Dicerorhinus* are not resolved.

Discussion

The validation of *P. ringstroemi* As we have presented above, the new material from the Linxia Basin provides important information of some key anatomical structures and their variation. Especially, the preservation of premaxillae in two crania suggests that the upper I1 of *P. ringstroemi* is large and has an oval shape. This is in contrast to the case of *Pliorhinus megarhinus* from Europe, whose incisor is very small (latest Miocene) (Pandolfi and Rook 2017) or possibly lost (Pliocene) (Gervais 1851). The size and presence or absence of incisors is generally viewed as important evidence to infer the evolution and taxonomy of rhinoceros, as it is correlated with feeding behavior, predator defence, and co-evolved with rhino horns (Guérin 1980; Qiu and Wang 2007). Subsequently, the clearly different evolutionary stages of eastern Asian material and those from Europe support a species-level difference between the two. In addition to this trait, the eastern Asian material is also different from *P. megarhinus* in having a more vertical anterior border of the ascending ramus of the mandible HMV2048. However, the latter differences are less obvious between the eastern Asian and European remains. In summary, our analyses suggest that *P. ringstroemi* is a valid species, closely related to *P. megarhinus* of Europe, as revealed also by our phylogeny. In comparison to *P. megarhinus*, it retained large incisors. Recently, a partial cranium from Qin Basin of Shanxi, China was described and

assigned to *P. ringstroemi* (Shi et al. 2023). However, this cranium has a smaller size than *P. ringstroemi* present in this study, and the nasal is smaller. Most importantly, its upper I2 is much smaller than the ones in the Linxia Basin. The stratigraphy and age of the rhino from the Qin Basin are not fully clear (Shi et al. 2023). We suggest this partial cranium does not represent *P. ringstroemi*, but a different and possibly more derived form, but this needs further test, especially a systematic comparison with unpublished "*Dicerorhinus*" from the Yushe Basin (Tedford et al. 1991).

The evolutionary trend of Dicerorhina As has been proposed by previous authors, the dicerorhine rhinos experience some overall changes through their evolution. The most significant change lies in the anterior part of the skull, exemplified by the nasal, premaxilla, and mandible. The nasal gets progressively elongated, and the nasal notch moves backward. In *Dih. schleiermacheri*, the anterior tip of the nasal is not extended over the premaxilla, the nasal notch only reaches the level of the P2, and the infraorbital foramen is located far behind this level. In *Dih. pikermiensis*, the nasal is slightly more extended, and the nasal notch is also more posteriorly extended, reaching the level of the P3, and the infraorbital foramen is located slightly posterior to this level. In *Pliorhinus* and more derived dicerorhines (i.e., *Stephanorhinus* and *Coelodonta*) the nasal is clearly longer than the premaxilla, and the nasal notch reaches the level of the P3/P4 or even at the P4. The infraorbital foramen is located at the same level as that of the nasal notch in *Pliorhinus* and *Stephanorhinus*, but in *Coelodonta* this foramen is more posteriorly located than the nasal notch. *Stephanorhinus* and *Coelodonta* share a nasal septum ossification of different degrees together with its fusion with the ventral ridge of the nasal bone, which represents the only cases within Rhinocerotini.

The premaxillae in dicerorhine rhinos are always well developed. In contrast, the upper incisors are gradually reduced in number and size. In *Dih. schleiermacheri* there are two upper incisors, being with the I1 large. In *P. ringstroemi* the I2 is lost, whereas the I1 is still large. The I1 becomes significantly smaller in *P. megarhinus*, and generally lost in *Stephanorhinus* (present in the earliest species *S. jeanvireti*) and *Coelodonta*. The lower incisor generally shows a similar pattern as the upper one.

The modern dicerorhine rhino *Dic. sumatrensis* is closest to *Dih. schleiermacheri* in having a short nasal, shallow nasal notch and large incisor, though the I2 is absent in the living species. *Dic. sumatrensis* is likely to be an early branch of dicerorhine rhinos as also revealed by our phylogeny, and retaining primitive traits in southeastern Asia during its whole evolutionary history.

Conclusion

The reported rhinoceros cranial remains from the Linxia Basin are identified as *Pliorhinus ringstroemi*. Morphological evidence from these specimens, especially based on the development of both premaxillae and incisors, supports *P. ringstroemi* as a valid species and sets it apart from the Mio-Pliocene *P. megarhinus*. The large sample allows some preliminary observations on intraspecific variation. Some traits, like the development of horn boss dorso-ventral curvature of nasal bone could be affected by gender and individual age. Our phylogeny supports *P. ringstroemi* is the sister group of two younger species of *Pliorhinus*. The modern *Dic. sumatrensis* is likely to be a conservative early branch of this lineage in regard to its nasal area morphology.

Supplementary information The online version contains supplementary material available at https://doi.org/10.1007/s10914-023-09698-w.

Acknowledgements We thank Second Comprehensive Scientific Expedition on the Tibetan Plateau for supporting the financial and logistical support in the field work. We thank J. Chen, W. He, S. Chen, L. Zhang for help in accessing fossil collections of the IVPP and HMV. We thank S. Liu and Y. Chen for artworks.

Author contributions Shijie Li wrote the main manuscript text and prepared figures, Oscar Sanisidro and Tao Deng contributed significantly to analysis and manuscript preparation. Shiqi Wang and Rong Yang helped perform the analysis with constructive discussions. All authors contributed to the conception of the study and reviewed the manuscript.

Funding The present study is supported in fossil repairation and field work by National Key Research and Development Program of China (grant number 2023YFF0804501), the Chinese Natural Science Foundation Program (grant number 42102001), Key Frontier Science Research Program of the Chinese Academy of Sciences (grant number QYZDY-SSW-DQC-22).

Data availability The datasets generated during and/or analysed during the current study are available in the text and supplementary online information files.

Declarations

Ethical statement The authors strictly followed ethical responsibilities.

Competing interests The authors declare no competing interests.

References

Abernethy AR (2011) Extreme variation in the sagittal crest of *Tapirus polkensis* (Mammalia Perissodactyla) at the Gray Fossil Site northeastern TN. Dissertation, Aaron Randall Abernethy

Adams DC, Otárola-Castillo E (2013) geomorph: an R package for the collection and analysis of geometric morphometric shape data. Methods Ecol Evol 4:393–399

Antoine P-O, Saraç G (2005) Rhinocerotidae (Mammalia, Perissodactyla) from the late Miocene of Akkasdagi, Turkey. Geodiversitas 27(4):601–632

Arambourg C (1959) Vertébrés continentaux da Miocène supérieur de l'Afrique du Nord. Service de la Carte géologique de l'Algérie Mémoire.
Baken EK, Collyer ML, Kaliontzopoulou A, et al. (2021) geomorph v4.0 and gmShiny: Enhanced analytics and a new graphical interface for a comprehensive morphometric experience. Methods Ecol Evol 12:2355–2363
Bibi F (2013) A multi-calibrated mitochondrial phylogeny of extant Bovidae (Artiodactyla, Ruminantia) and the importance of the fossil record to systematics. BMC Evol Biol 13:166
Chen G, Wu W-Y (1976) Mammalian fossils from the Miocene Jiulongkou locality, Cixian County, Heibei Province. Vertebr PalAsiat 14:6–15
Deng T (2004) A new species of the rhinoceros *Alicornops* from the Middle Miocene of the Linxia Basin, Gansu, China. Palaeontology 47:1427–1439
Deng T (2006) Neogene rhinoceroses of the Linxia Basin (Gansu, China). Cour Forsch-Inst Senckenberg 256:43–56
Deng T (2009) Late Cenozoic environmental changes in the Linxia Basin (Gansu, China) as indicated by cenograms of fossil mammals. Vertebr PalAsiat 47:282–298
Deng T, Hou S-K, Xie G-P, et al. (2013a) Chronostratigraphic subdivision and correlation of the Upper Miocene of the Linxia Basin in Gansu, China. J Stratigraphy 37:417–427
Deng T, Qiu Z, Wang B, et al. (2013b) Late Cenozoic biostratigraphy of the Linxia Basin, northwestern China. In: Wang XM, Flynn LJ, Fortelius M (eds), Neogene Terrestrial Mammalian Biostratigraphy and Chronology of Asia. Columbia University Press, New York, pp 243–273
Deng T, Wang X, Fortelius M, et al. (2011) Out of Tibet: Pliocene wooly rhino suggests high-plateau origin of ice age megaherbivores. Science 333:1285–1288
Geraads D (1988) Révision des Rhinocerotinae (Mammalia) du Turolien de Pikermi. Comparaison avec les formes voisins. Ann Paléontol 74:13–41
Gervais P (1851) Memoire sur le Rhinoceros fossile a Montpellier suivi de quelques remarques sur l'ensemble des mammiferes ongules. Memories de la Section des Sciences, Academie des Sciences et Lettres de Montpellier 2:59–79
Giaourtsakis IX (2003) Late Neogene Rhinocerotidae of Greece: distribution, diversity and stratigraphical range. In: Reumer JWF, Wessels W (eds), Distribution and Migration of Tertiary Mammals in Eurasia. Deinsea Rotterdam 10:235–253
Giaourtsakis IX (2022) The fossil record of rhinocerotids (Mammalia: Perissodactyla: Rhinocerotidae) in Greece. In: Vlachos E (ed), Fossil Vertebrates of Greece Vol. 2: Laurasiatherians, Artiodactyles, Perissodactyles, Carnivorans, and Island Endemics. Springer International Publishing, Cham, 409–500
Gilbert C, Ropiquet A, Hassanin A (2006) Mitochondrial and nuclear phylogenies of Cervidae (Mammalia, Ruminantia): Systematics, morphology, and biogeography. Mol Phylogenet Evol 40:101–117
Giribet G (2005) TNT: tree analysis using new technology. Syst Biol 54:176–178
Goloboff PA, Catalano SA (2016) TNT version 1.5, including a full implementation of phylogenetic morphometrics. Cladistics 32:221–238
Groves CP (1983) Phylogeny of the living species of rhinoceros. J Zoolog Syst Evol Res 21:293–313
Guérin C (1980) Les Rhinocéros (Mammalia, Perissodactyla) du Miocène terminal au Pléistocène supérieur en Europe occidentale. Comparaison avec les espèces actuelles. Documents du Laboratoire de Géologie, Université de Lyon, Sciences de la Terre 79:1−1184
Heissig K (1999) Family Rhinocerotidae. In: Rössner GE, Heissig K (eds) The Miocene Land Mammals of Europe. Pfeil, Munich, 175–188
Hillman-Smith AKK, Owen-Smith N, Anderson JL, Hall-Martin, AJ, Selaladi JP (1986) Age estimation of the white rhinoceros (*Ceratotherium simum*). J Zoology 210:355–379
Huelsenbeck JP, Ronquist F (2001) MRBAYES: Bayesian inference of phylogenetic trees. Bioinformatics 17:754–755
Johnson WE, Eizirik E, Pecon-Slattery J, et al. (2006) The late Miocene radiation of modern Felidae: a genetic assessment. Science 311:73–77
Li G, Davis BW, Eizirik E, et al. (2016) Phylogenomic evidence for ancient hybridization in the genomes of living cats (Felidae). Genome Res 26:1–11
Linden LV, Stoops K, Dumbá LCCS, et al. (2022) Sagittal crest morphology decoupled from relative bite performance in Pleistocene tapirs (Perissodactyla: Tapiridae). Integr Zool, 2023, 18(2):254–277
Liu S, Westbury MV, Dussex N, et al. (2021) Ancient and modern genomes unravel the evolutionary history of the rhinoceros family. Cell 184:4874–4885
Owen-Smith RN (1988) Megaherbivores. The Influence of Very Large Body Size on Ecology. Cambridge University Press, Cambridge. https://doi.org/10.1017/CBO9780511565441
Pandolfi L (2013) New and revised occurrences of *Dihoplus megarhinus* (Mammalia, Rhinocerotidae) in the Pliocene of Italy. Swiss J. Palaeontol 132:239–255
Pandolfi L (2023) Reassessing the phylogeny of Quaternary Eurasian Rhinocerotidae. J Quat Sci 38(3):1–4
Pandolfi L, Gasparik M, Piras P (2015) Earliest occurrence of *"Dihoplus" megarhinus* (Mammalia, Rhinocerotidae) in Europe (Late Miocene, Pannonian Basin, Hungary): Palaeobiogeographical and biochronological implications. Ann Paléontol 101:325–339
Pandolfi L, Pierre-Olivier A, Bukhsianidze M, et al. (2021) Northern Eurasian rhinocerotines (Mammalia, Perissodactyla) by the Pliocene–Pleistocene transition: phylogeny and historical biogeography. J Syst Palaeontol 19:1031–1057
Pandolfi L, Rook L (2017) Rhinocerotidae (Mammalia, Perissodactyla) from the latest Turolian localities (MN 13; Late Miocene) of central and northern Italy. Boll Soc Paleontol 56:45–56
Qiu ZX, Wang BY (2007) Paracerathere Fossils of China. Chinese Academy of Sciences, Beijing
Ringström T (1924) Nashörner der Hipparion-Fauna Nord-Chinas. Palaeontol Sinica C 1(4):1–156
Rohlf F (2010) tpsDIG2 Ver. 2.16. http://life.bio.sunysb.edu/morph/index.html
Ronquist F, Klopfstein S, Vilhelmsen L, et al. (2012a) A total-evidence approach to dating with fossils, applied to the early radiation of the hymenoptera. Syst Biol 61:973–999
Ronquist F, Teslenko M, van der Mark P, et al. (2012b) MrBayes 3.2: efficient Bayesian phylogenetic inference and model choice across a large model space. Syst Biol 61:539–542
Shi B-Z, Chen S-K, Lu X-K, et al. (2023) First report on rhinoceros from the late Neogene Qin Basin of Shanxi, China. Anat Rec: 1–9
Tedford RH, Flynn LJ, Qiu Z, et al. (1991) Yushe Basin, China: paleomagnetically calibrated mammalian biostratigraphic standard for the Late Neogene of Eastern Asia. J Vertebr Paleontol 11:519–526
Tedford RH, Wang X, Taylor BE (2009) Phylogenetic systematics of the north american fossil caninae (Carnivora: Canidae). Bull Am Mus Nat Hist 325:1–218
Tong H-w (2012) Evolution of the non-*Coelodonta* dicerorhine lineage in China. C R Palevol 11:555–562

Wickham H (2016) ggplot2: elegant graphics for data analysis. Springer, New York
Zhang C, Stadler T, Klopfstein S, et al. (2016) Total-evidence dating under the fossilized birth-death process. Syst Biol 65:228–249